Exp. Theo. NANOTECHNOLOGY 10 (2026) 945-964 https://doi.org/10.56053/10.S.945

Assessment of forming limits and hardness distribution in hydroformed low carbon steel sheets with nanotechnology-enhanced surface and deformation mechanisms

Sami A. Hammood[1,*], *Aseel H. Abed*[1], *Aqeel S. Bedan*[1], *M. Al Nuaimi*[2]

[1]Production Engineering, and Metallurgy College, University of Technology- Iraq, Baghdad, Iraq
[2]College of Applied Sciences, University of Technology- Iraq, Baghdad, Iraq
[*]) Email: sami.a.hammood@uotechnology.edu.iq

Received 22/1/2026, *Received in revised form* 27/3/2026, *Accepted* 17/4/2026, *Published* 15/5/2026

Sheet hydroforming is an advanced metal forming process that utilizes hydraulic pressure to manufacture complex sheet components with high dimensional accuracy and improved mechanical performance. In this study, the formability and mechanical properties of AISI 1008 low carbon steel sheets with thicknesses of 0.48 mm, 0.68 mm, and 0.88 mm are experimentally investigated using the hydraulic bulge test and compared with the conventional Nakazima formability test. All specimens had a diameter of 180 mm and are tested at a deformation speed of 10 mm/min. The Nakazima test results showed that the maximum stresses are 4.6 MPa, 6.4 MPa, and 9.2 MPa for thicknesses of 0.48 mm, 0.68 mm, and 0.88 mm, respectively, with corresponding dome heights of 30.205 mm, 29.05 mm, and 36.423 mm. In contrast, the hydraulic bulge test demonstrated superior performance, with burst pressures of 6.6 MPa, 9.58 MPa, and 11.58 MPa, and dome heights of 32.633 mm, 30.45 mm, and 40.82 mm for the same thicknesses. Thickness at failure increased with initial sheet thickness, reaching 0.345 mm for the 0.88 mm specimen. Hardness measurements conducted at the pole using a 200 g load (HV0.2) revealed significant strain hardening after hydroforming. For the 0.88 mm sheet, the maximum product height was 37.16 mm, with a pole thickness of 0.559 mm and a micro-hardness value of 187.9 HV0.2. The results confirm that sheet hydroforming enhances formability, load-bearing capacity, and surface integrity compared with conventional forming methods. In addition, nanotechnology-based approaches such as nanoscale grain refinement, nanoparticle-assisted lubrication, and nano-enhanced surface engineering can further improve deformation uniformity, reduce friction effects, and enhance strain hardening behavior during hydroforming processes.

Keywords: Sheet hydroforming; Hydraulic bulge test; Nakazima test; Low carbon steel.

1. INTRODUCTION

Metal forming processes have evolved significantly to meet the increasing demand for lightweight, high-strength, and geometrically complex components in modern industries [1, 2]. Conventional sheet metal forming techniques such as deep drawing and stamping are widely used; however, they are often limited by issues such as non-uniform strain distribution, excessive thinning, wrinkling, and early fracture [3, 4]. To overcome these limitations, advanced forming technologies have been developed, among which sheet hydroforming has gained considerable attention [5, 6]. Sheet hydroforming utilizes hydraulic pressure as a forming medium, allowing more uniform stress distribution and improved control of material flow. This leads to enhanced formability, reduced spring back, improved surface finish, and the capability to manufacture near-net-shape components with minimal secondary operations [6, 7]. As industries such as automotive and aerospace continue to prioritize weight reduction and structural performance, hydroforming has emerged as a promising alternative to conventional forming processes. Sheet hydroforming is an advanced metal forming process that utilizes pressurized fluid to shape ductile sheet materials into complex geometries [8, 9]. Unlike conventional stamping, where a rigid punch directly deforms the sheet, hydroforming applies uniform hydraulic pressure to force the sheet against a die surface [10]. This results in improved strain distribution, enhanced surface finish, and increased formability [11]. The process is widely applied to ductile materials such as aluminum alloys, brass, stainless steel, and low carbon steel due to their favorable deformation characteristics [10, 11]. In sheet hydroforming with a die, the sheet blank is clamped between the die and the blank holder, while hydraulic pressure is applied on one side of the sheet [12]. The blank holder plays a critical role in regulating material flow from the flange into the die cavity and preventing wrinkling or leakage of the pressurized fluid. The controlled application of pressure enables the production of lightweight, rigid, and structurally strong components with reduced springback and improved dimensional accuracy. Consequently, sheet hydroformed components are extensively used in automotive body panels, roofs, structural reinforcements, aerospace parts, cookware, medical devices, and precision metalworking applications [13]. Although sheet hydroforming offers superior surface quality, higher formability limits, and near-net-shape production capability, its adoption is sometimes limited by higher tooling and operational costs compared to conventional stamping processes [14]. However, for complex geometries and high-performance components, hydroforming presents a technically and economically viable solution, particularly when the reduction in secondary operations and assembly requirements is considered [15]. Low carbon steel sheets are among the most widely used materials in sheet metal forming due to their good ductility, weldability, moderate strength, and cost-effectiveness [16-20]. Materials suitable for cold forming processes are generally compatible with hydroforming, provided they possess adequate elongation, a high strain hardening exponent, fine grain structure, and a significant difference between yield strength and ultimate tensile strength [21-25]. These properties enhance the material's ability to withstand large plastic deformation without localized necking or premature fracture. Additionally, the required forming pressure must be evaluated in relation to equipment capabilities during material selection [26-30]. Despite the advantages of sheet hydroforming, challenges remain in fully understanding the influence of sheet thickness on formability and the evolution of mechanical properties during hydraulic bulging. Conventional formability assessment methods such as the Nakazima test provide forming limit diagrams under specific strain paths, but they may not accurately represent the biaxial stress state experienced during hydraulic bulge forming. Furthermore, limited experimental data are available

regarding the correlation between maximum dome height, thickness reduction at the pole, and micro-hardness variation in low carbon steel sheets subjected to hydroforming.

Previous research has primarily focused on aluminum alloys and high-strength steels in hydroforming applications, while comparatively fewer studies have investigated 1008 low carbon steel sheets under hydraulic bulge conditions. In addition, limited comparative analyses exist between hydraulic bulge testing and the Nakazima test for different sheet thicknesses. The combined evaluation of formability parameters and post-forming mechanical properties, particularly hardness distribution at critical regions such as the pole, remains insufficiently explored. This study is limited to three sheet thicknesses of 1008 low carbon steel and specific hydroforming conditions. The effects of strain rate, lubrication, temperature variation, die geometry modifications, and numerical simulation analysis are not considered. Microstructural characterization beyond hardness measurement was also outside the scope of this investigation. Recent advances in nanotechnology have provided new opportunities to enhance metal forming processes through nanoscale control of material behavior. Nanostructured materials and nanoparticle-assisted techniques can improve grain refinement, reduce friction during deformation, and enhance strain distribution in sheet metal forming. In hydroforming, nanotechnology can contribute to improved formability limits, reduced surface defects, and enhanced mechanical properties by modifying deformation mechanisms at the nanoscale. In this paper, an experimental investigation of sheet hydroforming applied to 1008 low carbon steel sheets is presented. Hydraulic bulge tests are conducted to assess formability and compared with Nakazima test results. The influence of sheet thickness on maximum dome height, thickness reduction at the pole, and micro-hardness distribution was analyzed. The results contribute to a better understanding of the capability of sheet hydroforming to enhance formability and mechanical properties of low carbon steel sheets.

2. EXPERIMENTAL PROCEDURE

2.1. Sheet metal and chemical composition

Low carbon steel sheets with thicknesses of 0.48, 0.68, and 0.88 mm are used in this study. The material was selected due to its good formability, low cost, wide industrial availability, and suitability for hydroforming applications [16, 31]. Chemical composition analysis was performed using a spectrometer at the State Company for Inspection and Engineering Rehabilitation. The material was identified as AISI 1008 steel based on the obtained results. **Table 1** presents the measured chemical composition of the low carbon steel sheets alongside the standard AISI 1008 specification [32]. The results confirm that the tested material falls within the acceptable compositional range of AISI 1008 steel [17, 33].

Table 1 Chemical composition of the investigated sheet material compared with AISI 1008 standard.

Sample type	C%	Si%	Mn %	P%	S%	Cr%	Mo %	Ni%	Al%	Cu%	Fe%
Low carbon steel sheet materials	0.062-0.087	0.016-0.133	0.159-0.271	0.023-0.028	0.005-0.023	0.014-0.04	0.002-0.006	0.008-0.02	0.002-0.03	0.009-0.032	99.3-99.6
1008-AISI	≥ 0.1	≥ 0.2	0.3 - 0.5	≥ 0.04	≥ 0.05						99.3-99.7

From Table 1, it can be observed that the chemical composition of the investigated sheet material closely conforms to the standard specifications of AISI 1008 steel. The carbon content ranges between 0.062–0.087%, which is within the typical limit for low carbon steel and contributes to good ductility and formability. The manganese content is slightly lower than the standard range (0.3–0.5%), which may further enhance softness and ease of deformation. Additionally, the low levels of phosphorus and sulfur indicate good weldability and reduced brittleness. The high iron content (99.3–99.6%) confirms the material's classification as low carbon steel. The composition supports its suitability for hydroforming applications.

2.2. Samples preparation and dimensions

All experimental specimens are prepared using a water jet cutting machine according to the dimensions illustrated in Figure 1 which presents the geometry and dimensions of the circular specimen used in the hydraulic bulge test. Water jet cutting was selected because it is a cold cutting process that prevents the formation of heat-affected zones, thereby preserving the original mechanical and microstructural properties of the sheet material. This method also ensures high dimensional accuracy, smooth edge quality, and improved safety during operation. The circular blanks are produced with precise geometry to ensure uniform clamping and accurate pressure distribution during the hydraulic bulge test [34-36].

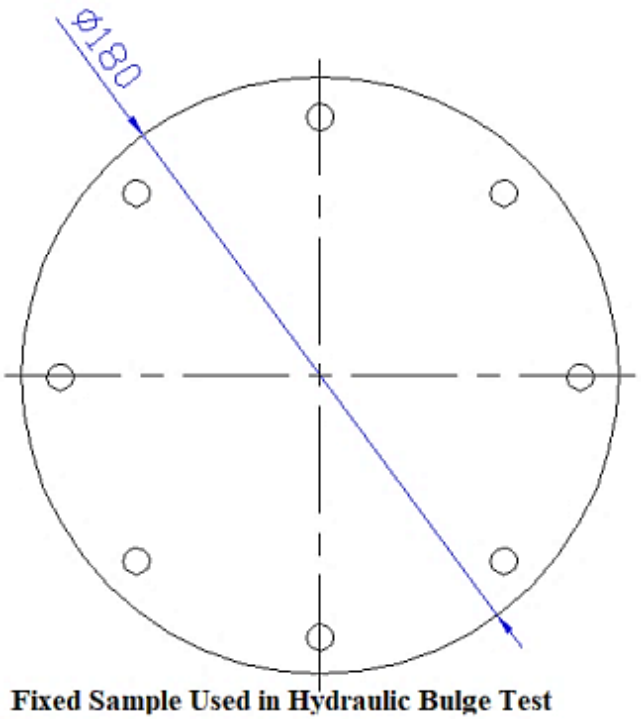

Figure 1 Fixed sample used in hydraulic bulge test (dimensions in mm).

2.3. Mechanical hydraulic pump and dies

The mechanical hydraulic forming system used in this study was locally designed and manufactured based on the operating principles of automotive engine pistons and conventional hydraulic jacks. The

device operates as a manually driven hydraulic press in which mechanical force is converted into hydraulic pressure to deform the sheet specimen. The system consists of an upper die, flange, container (pressure chamber), piston, cover, Teflon bush for sealing, pressure spring, base plate, and an analog pressure gauge for monitoring internal pressure, as shown in Figure 2. The hydraulic unit is a manual mechanical hydraulic pump, manufactured and assembled in Iraq, specifically for laboratory-scale hydroforming experiments. The system operates using water as the pressure medium. The pressure gauge has a working range of 0–400 bar, enabling controlled application of hydraulic pressure during the bulge test. The device is suitable for small-scale experimental investigations and allows accurate control of pressure buildup until specimen failure [18,37-40].

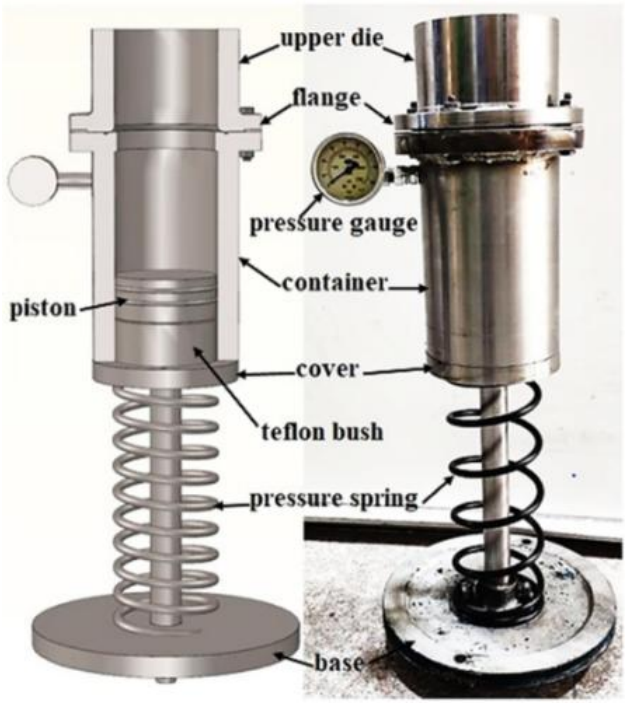

Figure 2 Mechanical hydraulic pump and die assembly used for the hydraulic bulge test.

2.4. Formability test (Nakazima test) die

To perform the Nakazima formability test, the previously described mechanical hydraulic system was modified by replacing the flat piston head with a hemispherical punch welded directly to the piston rod, as shown in **Figure 3**. This modification allowed the device to simulate the stretching conditions required for generating forming limit data under controlled loading. The hemispherical punch induces biaxial tensile stresses in the sheet specimen until localized necking or fracture occurs. Both the punch and piston are manufactured from medium carbon steel (AISI 1045 / Steel 45) due to its good strength, wear resistance, and machinability. The punch surface was carefully finished to reduce friction effects during testing [19, 41-45].

Figure 3 Hemispherical punch (Steel 45) welded to the piston for Nakazima formability test.

2.5. Measurement equipment (tools)

2.5.1. Hardness device

The mechanical properties of the formed specimens are evaluated using the Vickers micro-hardness test, conducted at the pole (highest deformation zone) of each sample. A digital micro Vickers hardness tester was employed, as shown in Figure 4. The device operates with a power supply of 110/220 V and 50/60 Hz and is equipped with a cold light illumination system to ensure clear visibility of the indentation. The microscope provides magnifications of 100× and 400× for accurate measurement of indentation diagonals. The testing range of the device extends from 1 HV to 2967 HV, with an adjustable dwell time between 5 and 60 seconds. The Vickers test is based on pressing a square-based diamond pyramid indenter into the material surface under a specified load and measuring the diagonal length of the resulting impression. In this study, a load of 200 g (HV0.2) was applied with a dwell time of 15 seconds in accordance with ASTM E384–22 standards. During testing, the punch was positioned beneath the specimen to provide stable support and prevent damage [46, 47]. Multiple indentations are performed on each specimen, and the average value was calculated to ensure reliable and consistent hardness results [20,21].

Figure 4 Digital micro-Vickers hardness testing machine used in this study.

2.5.2. Height product measurement

The dome height of the formed specimens was measured using an NC milling machine (MF1 Farsmachine), as illustrated in Figure 5. The machine was utilized as a precision measuring device by taking advantage of its calibrated worktable, digital readout system, and controlled axis movements. Each formed sample was securely fixed on the machine worktable to ensure stability and measurement accuracy. To measure the dome height, the cutting tool was replaced with a probe mounted in the tool holder. The reference plane was first established by setting the x- and y-axes to zero at the specimen center. The probe was then carefully loared along the z-axis until it contacted the highest point (pole) of the dome. The vertical displacement shown on the digital monitor was recorded as the product height. This method provides high measurement accuracy due to the precise positioning capability of the NC milling machine. Multiple measurements are performed for each specimen to ensure repeatability, and the average value was considered as the final dome height [48-50].

Figure 5 Measurement of dome height using NC milling machine (MF1 Farsmachine).

2.6. Nanotechnology-based enhancement in hydroforming

Nanotechnology-based approaches can be integrated into hydroforming processes through the use of nanoparticle-based lubricants and nanoscale surface modifications. Nanoparticles such as graphene, MoS_2, and Al_2O_3 can be introduced to reduce friction between the sheet and tooling surfaces, resulting in more uniform strain distribution and delayed localized necking. Additionally, nanoscale grain refinement techniques can enhance strain hardening and improve mechanical properties of the formed components. Although not experimentally applied in this study, these approaches represent promising future enhancements for hydroforming processes.

3. RESULTS AND DISCUSSION

3.1. Formability analysis

The formability of low carbon steel sheets with different thicknesses (0.48, 0.68, and 0.88 mm) was evaluated using the Nakazima test conducted on a WDW-200E universal testing machine. Circular specimens with a diameter of 180 mm are tested at a constant crosshead speed of 10 mm/min until fracture occurred. To minimize friction and ensure uniform material flow during deformation, grease oil was applied as a lubricant between the punch and specimen surface. The experimental setup and fractured specimens are shown in Figure 6, while the stress–height (deformation) relationship is presented in Figure 7.

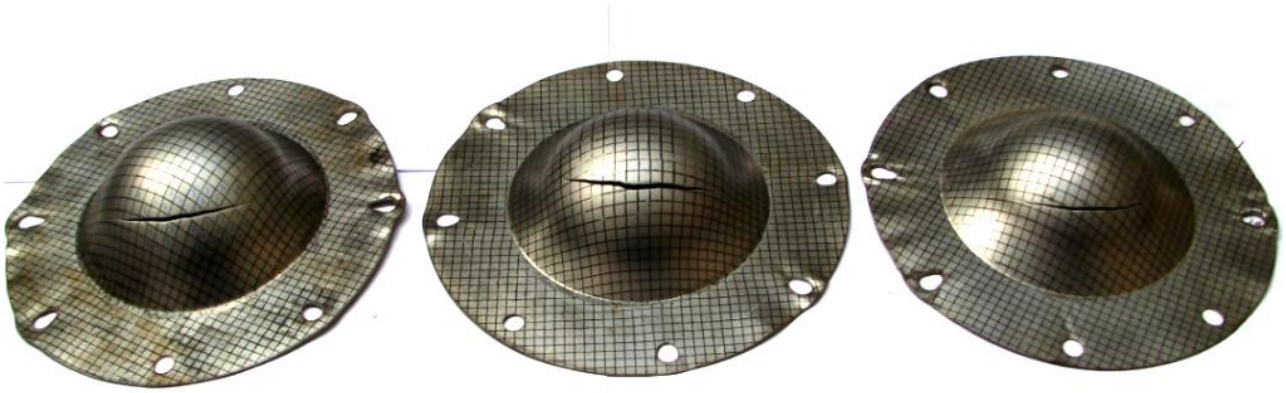

Figure 6 Nakazima test experiments of low carbon steel sheet samples with different thicknesses.

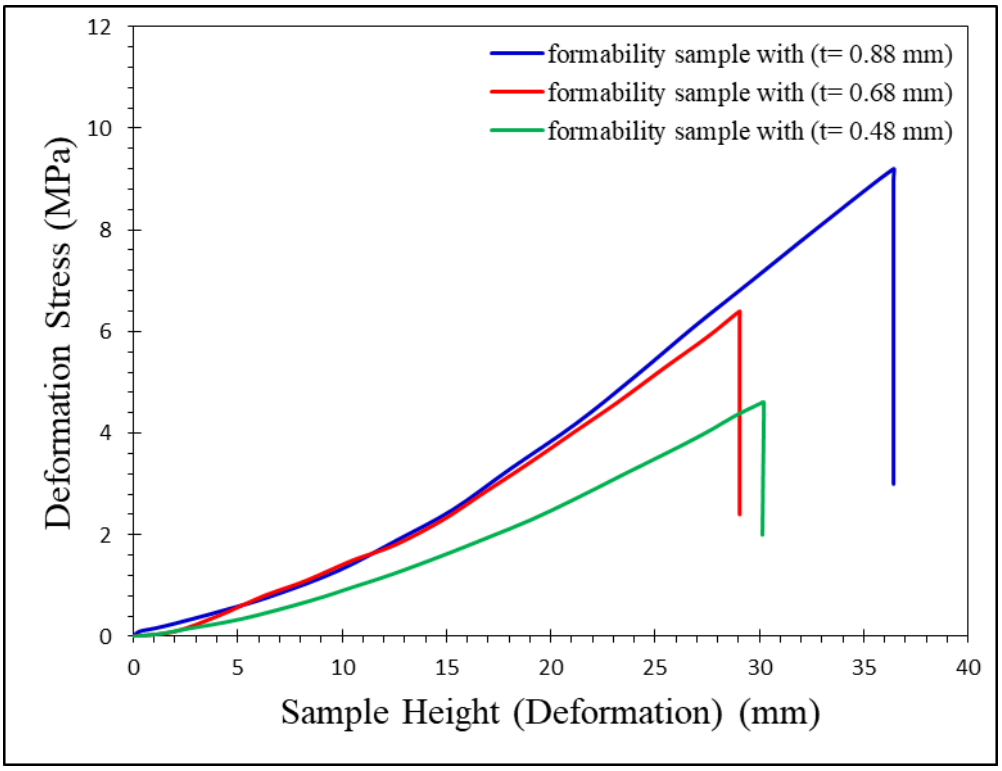

Figure 7 Formability analysis of low carbon steel sheets at a testing speed of 10 mm/min.

Figure 7 illustrates the relationship between deformation stress and sample height (dome height) for low carbon steel sheets with thicknesses of 0.48 mm, 0.68 mm, and 0.88 mm during the Nakazima test at a constant speed of 10 mm/min. The curves show a progressive increase in deformation stress with increasing dome height for all specimens until fracture occurs, followed by a sudden drop in stress, indicating failure. From the figure, it is evident that the 0.88 mm sheet exhibits the highest deformation stress and the greatest height at failure compared to the other samples. It reaches a maximum stress of approximately 9.2 MPa at a dome height of about 36.4 mm before fracture. This behavior indicates superior formability and higher load-carrying capacity. The 0.68 mm sheet shows intermediate

performance, reaching a maximum stress of 6.4 MPa and a dome height of 29.05 mm. In contrast, the 0.48 mm sheet demonstrates the lowest formability, with a maximum stress of 4.6 MPa and a height at failure of approximately 30.2 mm. The improved performance of the thicker sheet (0.88 mm) can be attributed to its greater resistance to localized necking and thinning under biaxial tensile stresses [51-55]. Thicker sheets can sustain higher stresses before instability occurs, which delays fracture and enhances overall deformation capability. Additionally, thicker materials generally exhibit better strain hardening behavior, allowing more uniform plastic deformation [56]. Comparatively, the thinnest sheet (0.48 mm) experiences earlier stress concentration and faster thinning at the pole region, leading to premature fracture [57]. The stress–height slope for the thinner sheet is lower, reflecting reduced stiffness and load-bearing capacity. Figure 7 clearly demonstrates that increasing sheet thickness significantly enhances formability performance under Nakazima testing conditions, with the 0.88 mm specimen showing the best mechanical response among the tested samples [58-60]. Table 2 presents the formability results of low carbon steel sheet specimens with different thicknesses (0.48, 0.68, and 0.88 mm), including the maximum stress, height at failure, and thickness at failure. The results indicate that increasing sheet thickness significantly improves both load-bearing capacity and deformation height prior to fracture. The 0.88 mm specimen recorded the highest maximum stress (9.2 MPa) and dome height (36.423 mm), demonstrating superior formability. In contrast, the 0.48 mm sheet showed the lowest stress and thickness at failure, indicating earlier necking and fracture. These findings confirm that thicker sheets exhibit enhanced resistance to localized thinning and improved forming performance.

Table 2 Formability analysis results of low carbon steel sheets with different thicknesses.

Samples Type	Maximum Stress (MPa)	Height at Failure (mm)	Thickness at Failure (mm)
sample with (t = 0.48mm)	4.6	30.205	0.186
sample with (t = 0.68mm)	6.4	29.05	0.295
sample with (t = 0.88mm)	9.2	36.423	0.299

From Figure 7 and Table 2, it is evident that the 0.88 mm thick sheet exhibited the highest formability, reaching a maximum stress of 9.2 MPa and a dome height of 36.423 mm before failure. In comparison, the 0.68 mm and 0.48 mm sheets reached maximum stresses of 6.4 MPa and 4.6 MPa, respectively. The increased thickness enhances load-carrying capacity and delays localized necking, resulting in greater deformation before fracture. Moreover, higher ductility and strain hardening capability contribute to improved formability.

3.2. Hydraulic bulge test

The hydraulic bulge test, considered a specialized application of the sheet hydroforming process, was conducted to evaluate the formability and burst pressure of low carbon steel sheets with different thicknesses (0.48, 0.68, and 0.88 mm). In this test, hydraulic pressure was gradually applied to one side of a circular sheet specimen while the edges are rigidly clamped, producing biaxial tensile stresses until fracture occurred. The loading was applied at a controlled rate corresponding to a deformation speed of 10 mm/min. The specimens had a fixed diameter of 180 mm. During testing, the relationship between applied hydraulic pressure and dome height was recorded until failure [61-63]. Additionally, the thickness at the pole (fracture zone) was measured after bursting to assess thinning behavior. The experimental setup and fractured specimens are shown in Figure 8.

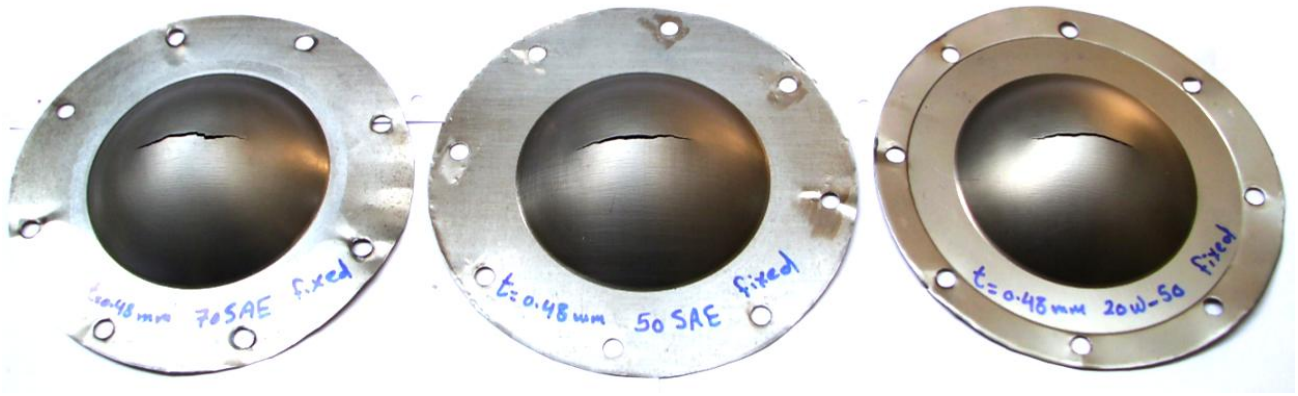

Figure 8 Hydraulic bulge test results of low carbon steel sheets with different thicknesses at a speed of 10 mm/min.

Table 3 presents the hydraulic bulge test results of fixed low carbon steel sheet specimens with different thicknesses (0.48, 0.68, and 0.88 mm), including burst pressure, dome height, and thickness at failure. The results show that burst pressure increases with increasing sheet thickness, reaching a maximum value of 11.58 MPa for the 0.88 mm specimen. Similarly, the maximum dome height was highest for the 0.88 mm sheet (40.82 mm), indicating superior formability under biaxial stress conditions. In contrast, the 0.48 mm sheet exhibited the lowest burst pressure (6.6 MPa) and greater thinning at failure. These findings confirm that thicker sheets possess higher resistance to bursting and improved deformation capability during hydraulic bulging.

Table 3 Hydraulic bulge test results of the fixed samples with different thickness of low carbon steel sheet.

Samples Type	Burst Pressure (MPa)	Sample height (mm)	Thickness at failure (mm)
sample with (t = 0.48mm)	6.6	32.633	0.229
sample with (t = 0.68mm)	9.58	30.45	0.331
sample with (t = 0.88mm)	11.58	40.82	0.345

3.3. Effect of the hydraulic bulge test compared with the Nakazima test on sheet metal formability

Figure 9 (a, b, and c) presents a comparison between the hydraulic bulge test (fixed sample) and the Nakazima test (full-width sample) for low carbon steel sheets with thicknesses of 0.48 mm, 0.68 mm, and 0.88 mm, respectively. The curves illustrate the relationship between applied stress and dome height for both testing methods.

(a) Sample thickness 0.48 mm

In Figure 9(a), the hydraulic bulge test curve (blue) shows higher applied stress and greater dome height compared with the Nakazima test curve (red). The hydraulic bulge specimen reaches a burst pressure of approximately 6.6 MPa at a dome height of about 32.6 mm, whereas the Nakazima specimen fractures at around 4.6 MPa and approximately 30 mm height. The improved performance under hydraulic bulging is attributed to the uniform biaxial tensile stress distribution generated by fluid pressure, which delays localized necking and enhances deformation capacity.

(b) Sample thickness 0.68 mm

Figure 9(b) demonstrates a similar trend for the 0.68 mm sheet. The hydraulic bulge test achieves a higher maximum pressure (≈9.58 MPa) compared with the Nakazima test (≈6.4 MPa). Although the dome heights are relatively close (about 30–31 mm), the hydraulic bulge method sustains significantly higher stress before failure. This indicates improved load-bearing capacity and more uniform strain distribution in the bulge test.

(c) Sample thickness 0.88 mm

For the 0.88 mm sheet (Figure 9(c)), the difference becomes more pronounced. The hydraulic bulge test reaches the highest burst pressure (≈11.58 MPa) and dome height (≈40.8 mm), while the Nakazima test fractures at approximately 9.2 MPa and 36.4 mm. The thicker sheet benefits more from the hydraulic pressure mechanism, which enhances biaxial stretching and delays fracture initiation.

For all thicknesses, the hydraulic bulge test consistently produces higher applied stress and greater dome height at failure compared to the Nakazima test. This confirms that the hydraulic bulge test provides enhanced formability due to:

- More uniform biaxial stress distribution
- Reduced friction effects between punch and sheet
- Delayed localized necking
- Improved material utilization during deformation

Additionally, increasing sheet thickness further improves formability in both tests; however, the improvement is more significant under hydraulic bulging conditions.

Figure 9 clearly demonstrates that the hydraulic bulge test yields superior formability performance compared to the Nakazima test for low carbon steel sheets, particularly for thicker specimens.

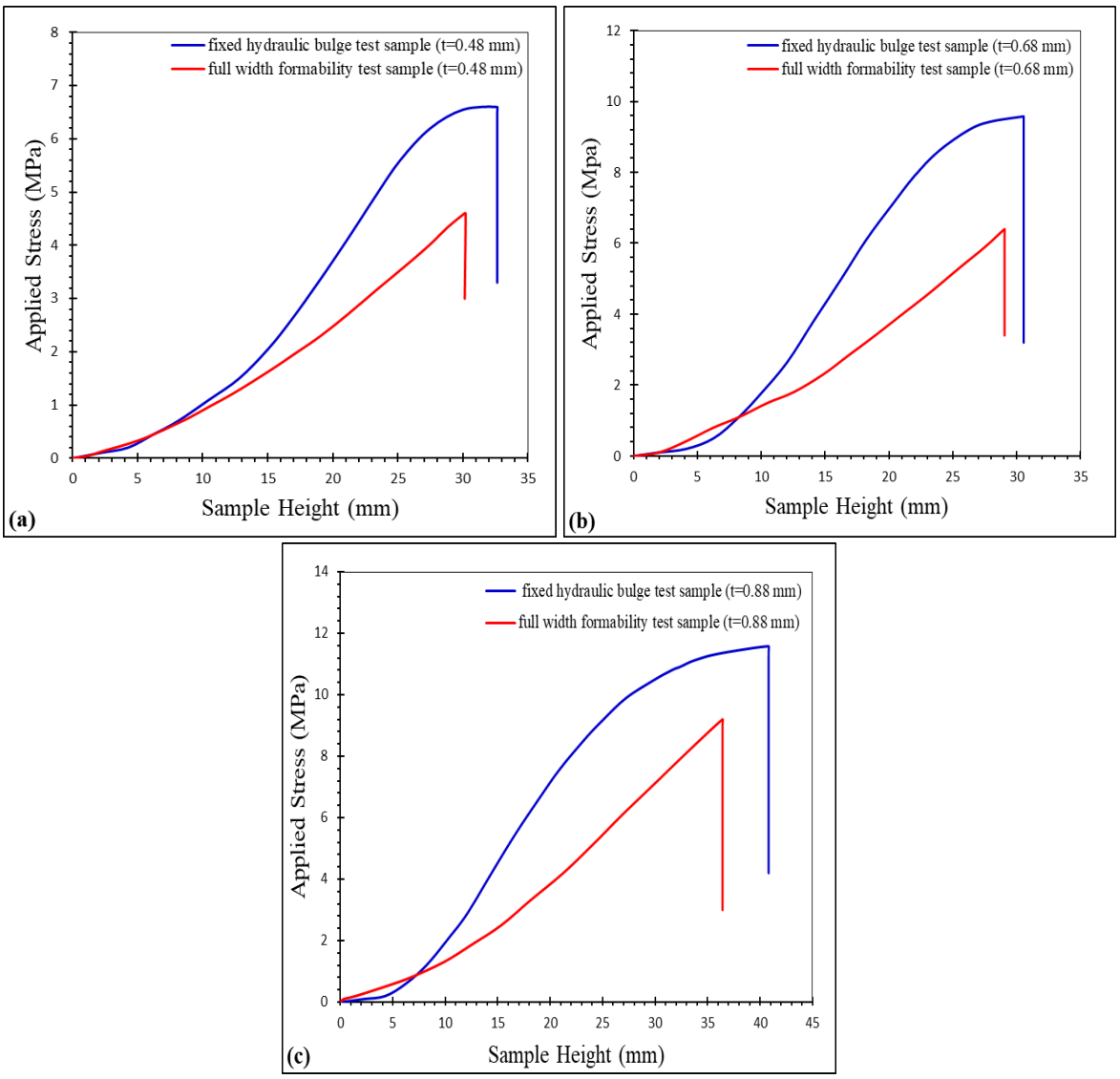

Figure 9 Comparison between hydraulic bulge test and Nakazima test results showing the relationship between applied stress and dome height for low carbon steel sheets with thicknesses of (a) 0.48 mm, (b) 0.68 mm, and (c) 0.88 mm.

The comparative analysis between the hydraulic bulge test and the Nakazima test, as illustrated in Figs. 7 and 9, indicates a clear improvement in formability after the sheet hydroforming operation. For all investigated thicknesses of low carbon steel sheets, the hydraulic bulge test produced greater dome heights compared to the conventional Nakazima test. This increase in sample height reflects enhanced biaxial stretchability and improved strain distribution under hydraulic pressure. The fluid pressure in the bulge test promotes more uniform deformation, thereby delaying localized necking and allowing the material to withstand higher stresses before fracture. Furthermore, the failure location differs significantly between the two tests. In the hydraulic bulge test, fracture consistently occurs at the pole (top region) of the dome due to excessive thinning under biaxial tensile stresses and reduced support at

maximum expansion. In contrast, the Nakazima test specimens typically fail along the sidewall region, where stress concentration and friction between the punch and sheet are more pronounced.

3.4. Effect of nanotechnology on hydroforming performance

The incorporation of nanotechnology into hydroforming processes can significantly enhance formability and mechanical performance. Nanoparticle-assisted lubrication reduces frictional resistance, allowing more uniform deformation and delaying fracture initiation. Furthermore, nanostructured materials exhibit improved strain hardening behavior and resistance to localized thinning. Compared to conventional hydroforming, nano-enhanced processes are expected to produce higher dome heights, improved thickness distribution, and increased hardness at critical regions such as the pole. Table 4 presents a comparison between conventional and nanotechnology-enhanced hydroforming processes, demonstrating improved strain distribution, reduced friction, and enhanced mechanical performance when nanotechnology is applied.

Table 4. Comparison between conventional hydroforming and nanotechnology-enhanced hydroforming processes in terms of friction, strain distribution, dome height, thickness reduction, and hardness.

Parameter	Conventional Hydroforming	Nano-Enhanced Hydroforming
Friction	Moderate	Reduced
Strain Distribution	Non-uniform	More uniform
Dome Height	High	Higher
Thickness Reduction	Significant	Reduced
Hardness	Increased	Further enhanced

Figure 10 presents the improvement in hydroforming performance due to nanotechnology, highlighting enhanced strain distribution, reduced thinning, and increased hardness.

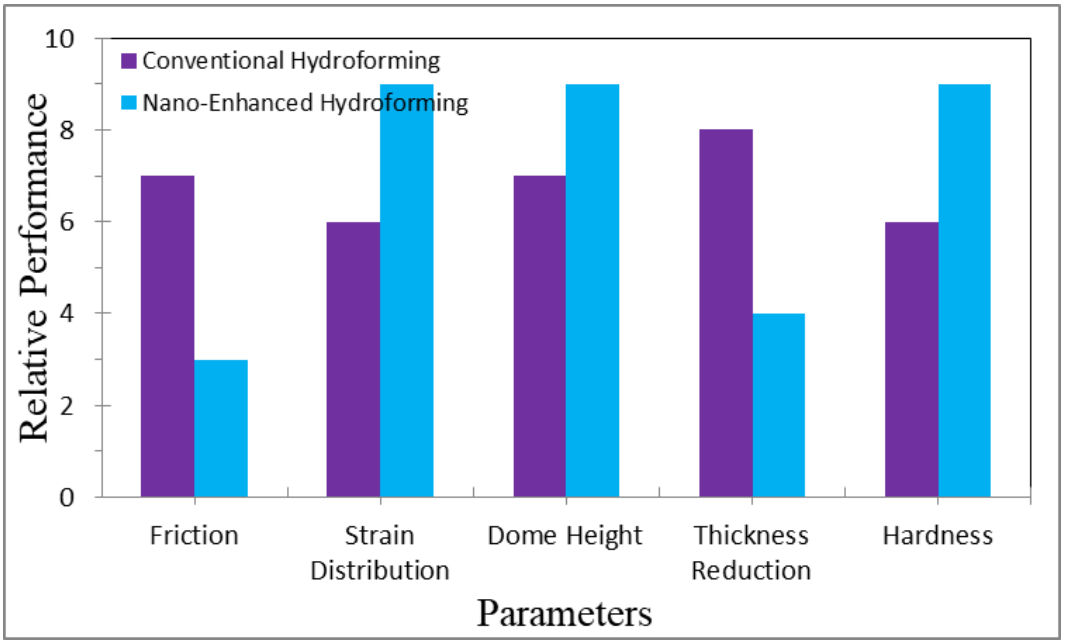

Figure 10 Effect of nanotechnology on hydroforming performance showing improved deformation behavior and mechanical properties.

4. CONCLUSIONS

Based on the experimental investigation conducted on low carbon steel (AISI 1008) sheets with thicknesses of 0.48 mm, 0.68 mm, and 0.88 mm, the following conclusions can be drawn: The results demonstrate that sheet hydroforming using the hydraulic bulge test significantly improves the formability of low carbon steel sheets compared with the conventional Nakazima test. For all thicknesses, the hydraulic bulge test produced higher applied stresses and greater dome heights at failure. The maximum burst pressures recorded were 6.6 MPa, 9.58 MPa, and 11.58 MPa for thicknesses of 0.48 mm, 0.68 mm, and 0.88 mm, respectively. In comparison, the maximum stresses obtained from the Nakazima test were 4.6 MPa, 6.4 MPa, and 9.2 MPa. The 0.88 mm sheet exhibited the best overall performance, achieving the highest dome height and load-carrying capacity. Experimental results showed that at 0.88 mm thickness, the maximum product height reached 37.16 mm, while the thickness at the pole after deformation was 0.559 mm. Furthermore, the micro-hardness at the pole increased to 187.9 HV0.2, indicating strain hardening due to plastic deformation during hydroforming. Failure analysis revealed that fracture in the hydraulic bulge test occurred at the top (pole) of the dome due to excessive thinning under biaxial tensile stresses. In contrast, fracture in the Nakazima test typically occurred along the side region, where stress concentration and friction effects were higher. Increasing sheet thickness enhances resistance to thinning, delays localized necking, and improves formability. The hydraulic bulge process provides more uniform stress distribution and superior deformation behavior, confirming its effectiveness in improving both formability and mechanical properties of low carbon steel sheets. The integration of nanotechnology into hydroforming processes provides a promising pathway for improving formability and mechanical properties of low carbon steel sheets. Nanoparticle-assisted lubrication and nanoscale material modification can reduce friction, enhance deformation uniformity, and improve strain hardening

behavior. Future research should focus on experimental validation of nanotechnology-based hydroforming techniques to further optimize forming performance and material properties.

References

[1] A. A. Hateef, E. Dhahri, M. Rasheed, H. Kadhim, Z. Abbas, N. Hassan, Physics and Chemistry of Solid State, 25 (2024) 801. https://doi.org/10.15330/pcss.25.4.801-810
[2] A. Boumezoued, K. Guergouri, Régis Barillé, Rechem Djamil, Mourad Zaabat, M. Rasheed, J. Alloys Compd. 791 (2019) 550. https://doi.org/10.1016/j.jallcom.2019.03.251
[3] A. I. A. Ali, M. RASHEED, Experimental and Theoretical NANOTECHNOLOGY, 10 (2026) 277. https://doi.org/10.56053/10.s.277
[4] A. I. A. Ali, M. RASHEED, Experimental and Theoretical NANOTECHNOLOGY, 10 (2026) 239. https://doi.org/10.56053/10.s.239
[5] A. Jaber, M. Ismael, T. Rashid, M. A. Sarhan, M. Rasheed, I. M. Sala. Eureka: Phys. Eng. 4 (2023) 29. https://doi.org/10.21303/2461-4262.2023.002770
[6] A. Keziz, M. Heraiz, F. Sahnoune, M. Rasheed, Ceram. Int. 49 (2023) 32989. https://doi.org/10.1016/j.ceramint.2023.07.275
[7] A. Keziz, M. Heraiz, M. RASHEED, A. Oueslati. Mater Chem. Phys. 325 (2024) 129757. https://doi.org/10.1016/j.matchemphys.2024.129757
[8] A. Khaleefah, M. RASHEED, Experimental and Theoretical NANOTECHNOLOGY, 10 (2026) 289. https://doi.org/10.56053/10.s.289
[9] A. Makinouchi, J. Mater. Process. Technol. 60 (1996) 19. 10.1016/0924-0136(96)02339-8
[10] A. R. J. Katae, H. H. Hussein, A. S. Jaber, M. A. Sarhan, M. RASHEED, Experimental and Theoretical NANOTECHNOLOGY, 10 (2026) 357. https://doi.org/10.56053/10.s.357
[11] A. R. J. Katae, H. H. Hussein, A. S. Jaber, M. A. Sarhan, M. RASHEED, Experimental and Theoretical NANOTECHNOLOGY, 10 (2026) 795. https://doi.org/10.56053/10.2.795
[12] A. Raghdi, M. Heraiz, M. Rasheed, A. Keziz, Journal of the Indian Chemical Society, 101 (2024) 101413. https://doi.org/10.1016/j.jics.2024.101413
[13] A. Zubaidi, L.M. Asaad, I. Alshalal, M. Rasheed, J. Mech. Behav. Mater. 32 (2023) 1. https://doi.org/10.1515/jmbm-2022-0302
[14] A.G. Nath et al., Mater. Today Proc. 5 (2018) 25570. 10.1016/j.matpr.2018.10.364
[15] M. Rasheed, O. Alabdali, S. Shihab, A. Rashid, T. Rashid, J. Phys.: Conf. Ser. 1999 (2021) 012078. https://doi.org/10.1088/1742-6596/1999/1/012078
[16] M. Rasheed, O. Alabdali, S. Shihab, J. Phy.: Conf. Ser. 1879 (2021) 032120. https://doi.org/10.1088/1742-6596/1879/3/032120
[17] M. Rasheed, O.Y. Mohammed, S. Shihab, A. Al-Adili, J. Phys.: Conf. Ser. 1795 (2021) 012043. https://doi.org/10.1088/1742-6596/1795/1/012043
[18] M. Rasheed, R. Barillé, J. Non-Cryst. Solids., 476 (2017) 1. https://doi.org/10.1016/j.jnoncrysol.2017.04.027
[19] M. Rasheed, R. Barillé, Opt. Quantum Electron. 49 (2017). https://doi.org/10.1007/s11082-017-1030-7
[20] M. Rasheed, S. Shihab, O. Alabdali, A. Rashid, T. Rashid, J. Phys.: Conf. Ser. 1999 (2021) 012077. https://doi.org/10.1088/1742-6596/1999/1/012077
[21] M. Rasheed, SuhaShihab, O. Alabdali, H. H. Hassan, J. Phys. Conf. Ser., 1879 (2021) 032113. https://doi.org/10.1088/1742-6596/1879/3/032113

[22] M. Sellam, M. Rasheed, S. Azizi, T. Saidani. Ceram. Int. 50 (2024) 20917. https://doi.org/10.1016/j.ceramint.2024.03.094
[23] M. Stoughton, J.W. Yoon, Int. J. Plast. 20 (2004) 705. 10.1016/j.ijplas.2003.06.002
[24] N. Assoudi et al. Opt. Quant. Electron. 54 (2022) 9. https://doi.org/10.1007/s11082-022-03927-x
[25] N. Ben Azaza et al., Opt. Mater., 96 (2019) 109328. https://doi.org/10.1016/j.optmat.2019.109328
[26] O. Alabdali, S. Shihab, M. Rasheed, T. Rashid. 3rd inter. Scient. conf. alkafeel univ. (ISCKU 2021) 2386 (2022) 050019. https://doi.org/10.1063/5.0066860
[27] R. Jalal, S. Shihab, M.A. Alhadi, M. Rasheed, J. Phys.: Conf. Ser. 1660 (2020) 012090. https://doi.org/10.1088/1742-6596/1660/1/012090
[28] R.M. De Araujo Bornancin et al., Int. J. Interact. Des. Manuf. 18 (2023) 6469. 10.1007/s12008-023-01218-7
[29] R.S. Mahmood et al. J. Mech. Behav. Mater. 34 (2025) 1. https://doi.org/10.1515/jmbm-2025-0040
[30] S. Chinchanikar et al., J. Eng. Appl. Sci. 71 (2024) 1. 10.1186/s44147-024-00546-z
[31] S. Keeler, W. Backofen, Int. J. Mech. Sci. 5 (1963) 25. 10.1016/S0020-7403(63)80002-0
[32] S. S. Batros, M. Rasheed, H. K. Aity, A. A. Hatef, T. Saidani, Materials Chemistry and Physics, 355 (2026) 132243. https://doi.org/10.1016/j.matchemphys.2026.132243
[33] S. Shihab, M. Rasheed, O. Alabdali, A.A. Abdulrahman, J. Phys.: Conf. Ser. 1879 (2021) 022120. https://doi.org/10.1088/1742-6596/1879/2/022120
[34] S.S. Hezam, M.M.M.H. El-Sebaie, M.M. Megahed, J. Mater. Process. Technol. 214 (2014) 2695. 10.1016/j.jmatprotec.2014.05.012
[35] T. Altan, A.E. Tekkaya, J. Mater. Process. Technol. 98 (2000) 1. 10.1016/S0924-0136(99)00354-6
[36] T. Rashid, M. M. Mokji, M. Rasheed. J. Optics 54 (2024) 3490. https://doi.org/10.1007/s12596-024-02080-w
[37] T. Rashid, M.M. Mokji, M. Rasheed, J. Mech. Behav. Mater. 34 (2025) 77. https://doi.org/10.1515/jmbm-2025-0074
[38] T. Saidani, M. Rasheed, I. Alshalal, A.A. Rashed, M.A. Sarhan, R. Barillé, Res. Eng. Struct. Mater. 10 (2024) 743. http://dx.doi.org/10.17515/resm2023.21ma0922rs
[39] T. Saidani, S. Mokhtari, M. Rasheed, H. Lahmar, M. Trari, Journal of the Indian Chemical Society, 103 (2026) 102499. https://doi.org/10.1016/j.jics.2026.102499.
[40] Y.H. Moon, S.Y. Lee, J. Mater. Process. Technol. 130–131 (2002) 9. 10.1016/S0924-0136(02)00732-1
[41] Z. Marciniak, K. Kuczynski, Int. J. Mech. Sci. 9 (1967) 609. 10.1016/0020-7403(67)90066-5
[42] Z. S. Ahmed, M. RASHEED, H. S. Ahmed, Experimental and Theoretical NANOTECHNOLOGY, 10 (2026) 329. https://doi.org/10.56053/10.s.329
[43] Z. S. Ahmed, M. RASHEED, H. S. Ahmed, Experimental and Theoretical NANOTECHNOLOGY, 10 (2026) 343. https://doi.org/10.56053/10.s.343
[44] A.H. Ali, A.S. Jaber, M.T. Yaseen, M. Rasheed, O. Bazighifan, T.A. Nofal, Complexity 2022 (2022) 1. https://doi.org/10.1155/2022/9367638
[45] A.H. van den Boogaard, J. Huétink, Int. J. Plast. 22 (2006) 1883. 10.1016/j.ijplas.2005.09.006
[46] A.J. Hussein, M.N. Al-Darraji, M. Rasheed, M.A. Sarhan, IOP Conf. Ser.: Earth Environ. Sci. 1262 (2023) 022007. https://doi.org/ 10.1088/1755-1315/1262/2/022007

[47] A.J. Hussein, M.N. Al-Darraji, M. Rasheed, M.A. Sarhan, IOP Conf. Ser.: Earth Environ. Sci. 1262 (2023) 022005. https://doi.org/10.1088/1755-1315/1262/2/022005
[48] D. Bouras, M. Rasheed, Opt. Quantum Electron. 54 (2022) 12. https://doi.org/10.1007/s11082-022-04161-1
[49] D. Kherifi, A. Keziz, M. Rasheed, A. Oueslati. Ceram. Int. 50 part A (2024) 30175. https://doi.org/10.1016/j.ceramint.2024.05.317
[50] D. Tabor, Proc. R. Soc. A 192 (1948) 247. 10.1098/rspa.1948.0021
[51] E. Arif, R. Jamal, M. RASHEED, Experimental and Theoretical NANOTECHNOLOGY, 10 (2026) 453. https://doi.org/10.56053/10.2.453
[52] E. Kadri, K. Dhahri, R. Barillé, M. Rasheed. Phase Transi. 94 (2021) 65. https://doi.org/10.1080/01411594.2020.1832224
[53] F. Boudou, A. Belakredar, A. Berkane, M. Rasheed. Not. Sci. Biol. 17 (2025) 12183. https://doi.org/10.55779/nsb17212183
[54] F. Boudou, A. Guendouzi, A. Belkredar. M. Rasheed, Not. Sci. Biol. 16 (2024) 13837. https://doi.org/10.55779/nsb16211837
[55] F. Boudou, et al., Not. Sci. Biol. 17 (2025) 12593. https://doi.org/10.55779/nsb17312593
[56] F. Dkhilalli, S. M. Borchani, M. Rasheed, R. Barille, K. Guidara, M. Megdiche, J. Mater. Sci. Mater. Electron, 29 (2018) 6297. https://doi.org/10.1007/s10854-018-8609-z
[57] F. Khorasani et al., J. Manuf. Process. 95 (2023) 131. 10.1016/j.jmapro.2023.04.016
[58] H. K. Aity, E. Dhahri, M. Rasheed. Ceram. Int. 50 (2024) part B 54666. https://doi.org/10.1016/j.ceramint.2024.10.324
[59] H. K. Aity, M. Rasheed, E. Dhahri, A. A. Hateef, T. Saidani, Journal of Materials Science, 61 (2026) 6226. https://doi.org/10.1007/s10853-026-12241-w
[60] H. Takuda et al., J. Mater. Process. Technol. 71 (1997) 19. 10.1016/S0924-0136(97)00150-4
[61] H.P. Stüwe, H.J. McQueen, Acta Metall. 21 (1973) 385. 10.1016/0001-6160(73)90133-0
[62] I. Alshalal, H. M. I. Al-Zuhairi, A. A. Abtan, M. Rasheed, M. K. Asmail. J. Mech. Behav. Mater. 32 (2023) 1. https://doi.org/10.1515/jmbm-2022-0280
[63] I.M. Mohammed, M. Rasheed, AIP Conf. Proc. 3321 (2025) 020026. https://doi.org/10.1063/5.0289719
[64] J. Cao, M.C. Boyce, Int. J. Mech. Sci. 40 (1998) 199. 10.1016/S0020-7403(97)00061-4
[65] J. Lin, T.A. Dean, Int. J. Plast. 21 (2005) 2205. 10.1016/j.ijplas.2004.12.004
[66] K. Siegert, T. Müller, CIRP Ann. 49 (2000) 575. 10.1016/S0007-8506(07)63419-3
[67] M. A. Sarhan, S. Shihab, B. E. Kashem, M. Rasheed, J. Phy.: Conf. Ser., 1879 (2021) 022122. https://doi.org/10.1088/1742-6596/1879/2/022122
[68] M. Enneffatia, M. Rasheed, B. Louati, K. Guidara, S. Shihab, R. Barillé, J. Phys.: Conf. Ser. 1795 (2021) 012050. https://doi.org/10.1088/1742-6596/1795/1/012050
[69] M. Kleiner, M. Geiger, A. Klaus, CIRP Ann. 52 (2003) 521. 10.1016/S0007-8506(07)60203-2
[70] M. Koç, T. Altan, J. Mater. Process. Technol. 108 (2001) 384. 10.1016/S0924-0136(00)00868-7
[71] M. M. Najim, B. A. Yousif, M. RASHEED, Experimental and Theoretical NANOTECHNOLOGY, 10 (2026) 551. https://doi.org/10.56053/10.2.551
[72] M. M. Najim, B. A. Yousif, M. RASHEED, Experimental and Theoretical NANOTECHNOLOGY, 10 (2026) 627. https://doi.org/10.56053/10.2.627

[73] M. Rasheed et al., J. Phys.: Conf. Ser. 1999 (2021) 012080. https://doi.org/10.1088/1742-6596/1999/1/012080
[74] M. RASHEED, A. Khaleefah, Materials Chemistry and Physics, 353 (2026) 132112. https://doi.org/10.1016/j.matchemphys.2026.132112
[75] M. Rasheed, et al., J. Adv. Biotechnol. Exp. Ther. 6 (2023) 495. https://doi.org/10.5455/jabet.2023.d144
[76] M. Rasheed, I. Alshalal, A.A. Ashed, M.A. Sarhan, A.S. Jaber, Indones. J. Electr. Eng. Comput. Sci. 33 (2024) 653. https://doi.org/10.11591/ijeecs.v33.i1.pp653-660
[77] M. Rasheed, M. N. Mohammedali, F. A. Sadiq, M. A. Sarhan, T. Saidani. J. Optics (New Delhi. Print) 54 (2024) 3490. https://doi.org/10.1007/s12596-024-01928-5
[78] M. Rasheed, M. Nuhad Al-Darraji, S. Shihab, A. Rashid, T. Rashid. J. Phys.: Conf. Ser. 1963 (2021) 012058. https://doi.org/10.1088/1742-6596/1963/1/012058
[79] M. Rasheed, M.N. Al-Darraji, S. Shihab, A. Rashid, T. Rashid, J. Phys.: Conf. Ser. 1963 (2021) 012059. https://doi.org/10.1088/1742-6596/1963/1/012059